PHYSICAL REVIEW B **85**, 085111 (2012)

Unusually long free carrier lifetime and metal-insulator band offset in vanadium dioxide

Chris Miller,[1] Mark Triplett,[1] Joel Lammatao,[1] Joonki Suh,[2] Deyi Fu,[2,3] Junqiao Wu,[2] and Dong Yu[1,*]

[1]*Department of Physics, University of California, Davis, California 95616, USA*

[2]*Department of Materials Science and Engineering, University of California, Berkeley, California 94720, USA*

[3]*Jiangsu Provincial Key Laboratory of Advanced Photonic and Electronic Materials, School of Electronic Science and Engineering, Nanjing University, Nanjing 210093, China*

(Received 14 December 2011; published 15 February 2012)

Single crystalline vanadium dioxide (VO_2) nanobeams offer an ideal material basis for exploring the widely observed insulator–metal transition in strongly correlated materials. Here, we investigate nonequilibrium carrier dynamics and electronic structure in single crystalline VO_2 nanobeam devices using scanning photocurrent microscopy in the vicinity of their phase transition. We extracted a Schottky barrier height of ∼0.3 eV between the metal and the insulator phases of VO_2, providing direct evidence of the nearly symmetric band gap opening upon phase transition. We also observed unusually long photocurrent decay lengths in the insulator phase, indicating unexpectedly long minority carrier lifetimes on the order of microseconds, consistent with the nature of carrier recombination between two d-subbands of VO_2.

DOI: 10.1103/PhysRevB.85.085111 PACS number(s): 71.30.+h, 72.20.Jv, 73.30.+y

I. INTRODUCTION

Vanadium dioxide (VO_2) is one of the most studied strongly correlated materials. VO_2 undergoes a first-order insulator–metal transition (IMT) at $T_c = 68\,^{\circ}C$,[1] which involves a drastic change in both electric resistivity and crystal structure. In its insulating (I) phase ($T < T_c$), VO_2 has a monoclinic crystal structure with a band gap of ∼0.6 eV,[2] which transforms into a tetragonal structure in its metallic (M) phase at higher temperatures ($T > T_c$) [Fig. 1(a)]. The electronic structure at the junction of M-I domain walls in VO_2 is of great interest to understanding the mechanism of IMT but has rarely been directly explored. Intriguing questions remain unanswered, such as how the bands line up between the two phases, whether the interface is ohmic or Schottky, and how much the bands bend at the interface. The answers to these questions can shed light on the IMT mechanism in strongly correlated materials, which is still under debate in the case of VO_2 after decades of studies.[3,4] In addition, the charge carrier diffusion lengths have not yet been measured in VO_2. Combined with mobilities measured by Hall or field effect, charge carrier lifetimes can be extracted from the diffusion lengths to elucidate the charge carrier dynamics. The difficulties of measuring charge carrier lifetimes in VO_2 partly result from its inability for light emission, which prevents time-resolved luminescence studies, and its unintentional phase transition during pump-probe measurements. Random M-I domain structures that typically occur in VO_2 thin films or bulk specimens also complicate spatially resolved electric measurements.[5] Recently, single crystalline VO_2 nanobeams (NBs) with a rectangular cross section have been successfully synthesized via a vapor transport approach.[6] These VO_2 NBs provide an excellent platform for investigating the electronic structure at the M-I junction (domain wall); the characteristic domain size is larger than the lateral dimension of the NB, so a simple 1D domain structure can be easily stabilized in the axial direction of the NB.

II. METHODS

Scanning photocurrent microscopy (SPCM) is an ideal technique for extracting a number of physical properties from quasi-one-dimensional (quasi-1D) structures, including electric field distribution, local band bending, barrier heights, and carrier diffusion lengths.[7–13] A typical SPCM experiment involves rastering a diffraction limited laser spot over a planar device while recording the photocurrent as a function of the local carrier injection position. Spatially resolved photocurrents in VO_2 NBs have been measured previously[14] but only at very high laser intensity (on the order of 250 kW/cm^2), where the photocurrent is dominated by the thermoelectric effect. In this work, we use laser intensities 1000 times weaker than the previous report to probe intrinsic carrier dynamics by ensuring that the photoinjection does not induce unintentional phase transitions and significant temperature gradients. At this low intensity, the local temperature rise due to laser heating is estimated to be on the order of a kelvin, and we conclude as seen below that the thermoelectric effect can be ignored. We found that the energy band in the *n*-type I phase bends upward toward the M phase with a barrier height of ∼0.3 eV. More interestingly, we observed unexpectedly long minority carrier (hole) diffusion lengths in the I phase, indicating long carrier lifetimes on the order of microseconds.

The VO_2 NBs were grown by a physical vapor deposition approach in a horizontal tube furnace, as detailed in Ref. 6. Devices incorporating single VO_2 NBs were fabricated by photolithography on the as-grown substrates, where the NBs were partially embedded in the 1.1-μm-thick SiO_2 layer on Si wafers. Cr/Au contacts were thermally evaporated, creating 20-μm-gap devices with NBs that typically had a rectangular 1-μm^2 cross section. A scanning electron microscope (SEM) image of a typical device is shown in Fig. 2(b). The VO_2 NB devices showed linear current–voltage (I-V) characteristics with contact resistance much lower than the NB resistance, confirmed by four-probe measurements. The I phase VO_2 NBs were n-type with a relatively low electric resistivity of

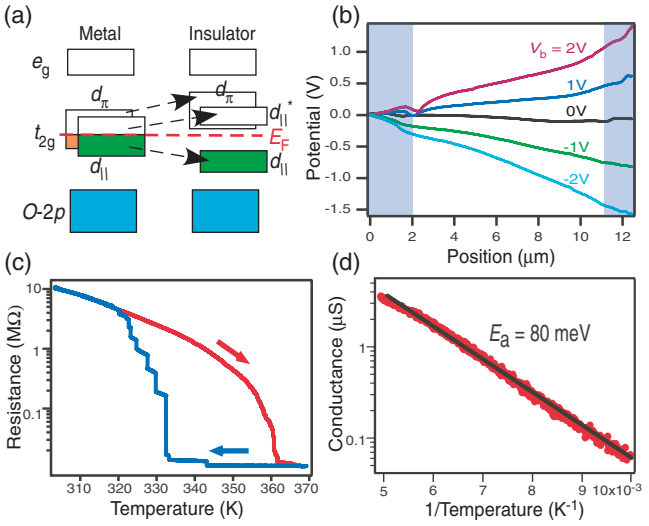

FIG. 1. (Color online) (a) Band diagram for M and I phases of VO_2, showing the splitting of the $d_{||}$-band and the rising of the d_π-band upon transition from the tetragonal (M) to monoclinic (I) crystal structures. (b) Kelvin probe microscopy measurement of a VO_2 NB at room temperature. Shaded areas indicate electrodes. (c) Resistance as a function of temperature for a typical VO_2 NB device (D1). Arrows indicate the temperature ramping directions. (d) Conductance as a function of inverse temperature showing an activation energy of 80 meV.

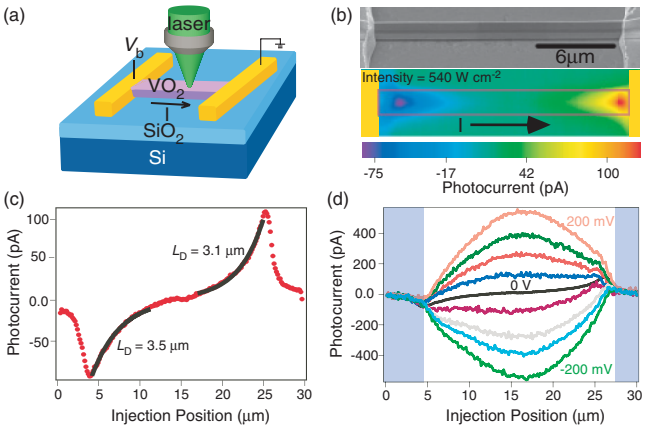

FIG. 2. (Color online) (a) Schematic of the SPCM setup, where a diffraction limited laser spot is rastered over a VO_2 NB device. (b) SEM image and SPCM image of a VO_2 NB at zero bias with an illumination intensity of 540 W cm^{-2} and wavelength of 532 nm (device D1). The arrow indicates the positive current direction. (c) Cross section of the SPCM image in (b) in the axial direction of the NB. The data are fit to the exponential form $I = I_0 \exp[-(x - x_0)/L_D]$. The fitting parameters L_D are labeled in the plot. (d) SPCM line scans under biases ranging from −200 to 200 mV with 50-mV increments. The dark current was subtracted.

~5 Ω·cm. The kelvin probe microscopy showed that the electric potential was uniformly distributed along a typical NB at room temperature [Fig. 1(b)], indicating the NBs were free of defects that might induce a local electric field. The slight nonlinear evolution of the voltage profile near the contacts is likely due to the Schottky barriers between the VO_2 NB and the metal electrodes. The spatial resolution of our kelvin probe microscopy is on the order of 100 nm, longer than the expected depletion width, and thus cannot provide a direct measure of this width. As the temperature increased and M domains formed in the NBs, the device resistance decreased in discrete steps. A typical resistance–temperature curve can be seen in Fig. 1(c). The temperature-dependent conductance of a typical NB device followed the Arrhenius behavior well with an activation energy of 80 meV [Fig. 1(d)], much smaller than the band gap, indicating the NBs were highly doped.

Our SPCM setup was based on an Olympus 51× microscope, where a laser beam (continuous wave 532 nm, Compass 315M) was focused by a 100× numeric aperture 0.95 objective to a Gaussian profile with a full width at half maximum of 900 nm. Great care was taken to ensure that the laser intensity was well below the phase transition threshold, which is ~20 kW/cm^2 at room temperature. Thanks to the drastic difference in reflectivity, M domains can be visualized from optical images.[15] During laser scanning, we constantly checked the NBs optically to ensure no changes in domain configuration occurred. If our laser intensity was above the threshold, we observed the creation of an M domain at the injection position, and the M domain moved following the laser spot during the scanning.

III. RESULTS AND DISCUSSIONS

We first present the SPCM results of a typical single VO_2 NB device (D1) at room temperature (Fig. 2), far from the phase transition temperature (68 °C). The excitation laser peak intensity was 540 W/cm^2, much lower than the phase transition threshold; thus, the NB was completely in the I phase during scanning. A typical SPCM image at zero bias is shown in Fig. 2(b), displaying a significant photocurrent only when the illumination is near the contacts. The Schottky junction at the Cr contact leads to a zero-bias photocurrent,[11] and the current direction indicates an upward band bending toward the electrodes. In the more than 10 devices measured to date, the bending directions have been consistent and agree with the *n*-type nature of VO_2. An external quantum efficiency (ratio of collected carriers to incident photons) of 0.006% is estimated from the maximum zero-bias photocurrent (~100 pA) and the excitation intensity (540 W/cm^2). In addition, the current decays exponentially as the laser spot moves away from the contact, with a characteristic length of ~3 μm [Fig. 2(c)].

The photocurrent generated by local excitation in the I phase is unlikely to be caused by the thermoelectric current for the following reasons. First, when the laser spot is near the contact, only a small temperature rise on the order of 0.01 K is estimated at the VO_2/Au thermocouple junction because of the high thermal conductivity of Au. Such a small temperature difference leads to an ignorable thermoelectric current. Second, when the laser spot is near the center of the NB, the expected temperature increase is on the order of 1 K at the local illumination position. At first glance, this temperature rise seems to lead to a thermoelectric current high enough to account for the measured current level, considering a large Seebeck coefficient of the I phase of 0.4 mV/K.[16] However, the temperature at the left and right Au contacts remains

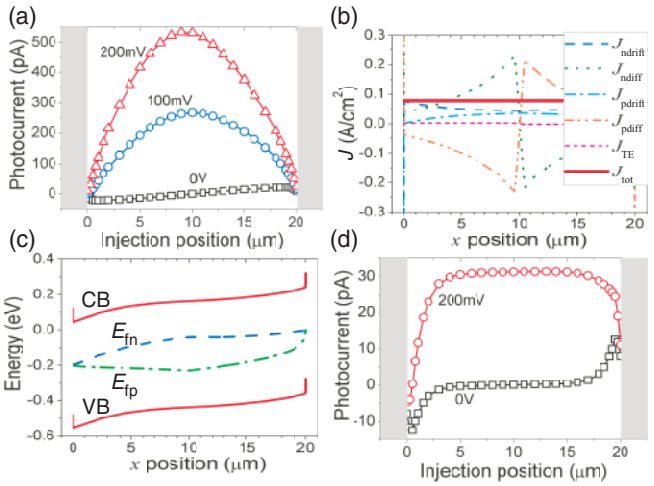

FIG. 3. (Color online) (a) Numerically simulated photocurrent of a VO_2 NB using the parameters summarized in the Table I scenario A. Bias voltages are 0, 100, and 200 mV, as labeled. The dark current was subtracted. (b) Simulated steady-state density of total current and current components when the laser is focused at 10 μm. J_{ndrift}, J_{ndiff}, J_{pdrift}, J_{pdiff}, J_{TE}, and J_{tot} are the electron drift current, electron diffusion current, hole drift current, hole diffusion current, thermoelectric current, and total current, respectively. (c) Band diagram corresponding to (b). CB, VB, E_{fn}, and E_{fp} are the conduction band minimum, valence band maximum, electron quasi-Fermi level, and hole quasi-Femi level, respectively. (d) Numerically simulated photocurrent of a VO_2 NB using the parameters summarized in Table I scenario B (shorter lifetimes). Bias voltages are 0 and 200 mV, as labeled.

at room temperature. The thermoelectric potential difference between the laser spot and the left contact is opposite that between the laser spot and the right contact. Thus, the thermoelectric current flowing toward the left-hand side of the laser spot largely cancels the thermoelectric current flowing toward the right-hand side, leading to a small net thermoelectric current. A numerically simulation shows that the thermoelectric current is much smaller than the measured current and can be ignored [J_{TE} in Fig. 3(b)].

The photocurrent decay may also be attributed to the decay in drift current driven by the built-in field in the depletion region at the weak Schottky contacts. However, the depletion region is expected to be less than 100 nm in the I phase, considering a dielectric constant of 24 and a high electron density of $\sim 10^{18}$ cm^{-3}.[4,17] Thus, the built-in field in the depletion region is unable to cause the long spatial extension of the photocurrent spots. As recently shown in a thorough modeling of SPCM,[18] carrier diffusion in conjunction with a weak Schottky field can cause a SPCM decay length much longer than the depletion width. Photogenerated carriers can diffuse to the depletion region, be separated by the built-in field at that location, and then be collected by the electrodes. The photocurrent decreases exponentially with the distance x away from the junction $\left(I = I_0 \exp(-x/L_{\text{D}})\right)$, as a longer distance results in a smaller fraction of carriers diffusing to the junction and being collected. The excellent exponential fits of our photocurrent data support the validity of this diffusion mechanism. SPCM is widely regarded as a powerful tool for determining the minority carrier diffusion length.[8,12,13] Following the Einstein relationship, the photocurrent decay length of $L_{\text{D}} = \sqrt{D_{\text{p}}\tau_{\text{p}}} = 3.3$ μm corresponds to a product of hole mobility (μ_{p}) and lifetime (τ_{p}) of $\mu_{\text{p}}\tau_{\text{p}} = 4.2 \times 10^{-6}$ cm^2/V. The mobility of the majority carriers (electrons) in n-type VO_2 NBs has been reported to be in the range of 0.1–1.0 cm^2/Vs in the insulator phase.[19] The minority carriers (holes) in the valence band are expected to have comparable or lower mobilities. If taking an upper bound of $\mu_{\text{p}} = 1$ cm^2/Vs for the I phase, a hole lifetime of $\tau_{\text{p}} \approx 4$ μs is expected for free holes. A lower μ_{p} yields an even longer lifetime. The rise/fall time of the photocurrent was measured to be 15 μs as the illumination was turned on/off (see supplementary material, Fig. S1).[20] This measured response time was limited by the instrumental temporal resolution. Thus, we conclude that the hole lifetime is $\tau_{\text{p}} = 4-15$ μs.

When a bias up to 200 mV is applied to the NB, the photocurrent is suppressed (enhanced) at the anode (cathode) [Fig. 2(d)], because the external electric field at the anode (cathode) is against (along with) the Schottky field. Besides this photocurrent change at the contacts, the most apparent change of the photocurrent profile under bias is an additional broad peak with higher magnitude appearing around the center of the NB. The dark current is already subtracted in Fig. 2(d). All devices measured to date show the same trend. However, the photocurrent spots in PbS nanowires[12] and Ge nanowires[21] are always close to one of the contacts under bias. This photocurrent under bias is another indication that the minority carrier lifetime is exceptionally long in VO_2, as shown by comparison with simulations. Following the method described in Ref. 22, we performed a numerical simulation of the electrodynamics of free carriers in 1D NBs under steady-state local illumination. The parameters used for the simulation are summarized in Table I. The nonequilibrium electrons and holes are generated solely in the illumination area, while they recombine throughout the entire NB.

TABLE I. Physical parameters used in the numerical simulation in Fig. 3.

Scenario	Band gap (eV)	N-type doping (cm^3) (Ref. 17)	Mobility (cm^2/Vs) (Ref. 19)	Lifetime (μs)	Effective mass (m_0) (Ref. 4)	Laser wavelength (nm)	Laser intensity (W/cm^2)	Barrier height (eV)
A	0.6	10^{18}	$\mu_{\text{n}} = 0.5$ $\mu_{\text{p}} = 0.5$	$\tau_{\text{n}} = 10$ $\tau_{\text{p}} = 10$	$m_{\text{n}} = 60$ $m_{\text{p}} = 60$	532	540	0.32
B	0.6	10^{18}	$\mu_{\text{n}} = 0.5$ $\mu_{\text{p}} = 0.5$	$\tau_{\text{n}} = 0.5$ $\tau_{\text{p}} = 0.5$	$m_{\text{n}} = 60$ $m_{\text{p}} = 60$	532	540	0.32

The simulation shows that for a given 1D system with zero- or low-energy barriers at the electrodes, weak local illumination typically generates nonequilibrium carriers ($\Delta n = \Delta p$) at much lower densities than the equilibrium majority carrier density ($n_0 = N_d$) coming from intentional or unintentional doping [Fig. S2(b)].[20] In this "low-level" injection, the photocurrent is very weak and has a flat line shape, with no discernible peak, as shown in Fig. 3(d). This is because the nonequilibrium carriers cannot reach the electrodes unless the laser injection spot approaches one of the electrodes. However, when the minority carrier lifetime (τ_p) is microseconds long, even weak illumination could generate nonequilibrium carrier densities much higher than in equilibrium, $\Delta n = \Delta p \gg n_0$, thus becoming effectively "high-level" injection [Fig. S2(a)].[20] This is because the recombination rate is low enough to allow a high density of nonequilibrium carriers to accumulate in the steady state. At a high-level injection, the photocurrent develops a broad peak under bias, and the peak is located where the total current switches from being limited by the electron current (electrons reaching the anode) to being limited by the hole current (holes reaching the cathode).[8] When the mobility and the lifetime of electrons are comparable to those of the holes, the photocurrent peak is located near the center of the NB, which is the case of the VO_2 NBs. Fig. 3(a) shows the simulated photocurrent profile in this case, which agrees well with the experimental data [Fig. 2(d)]. Also plotted in Figs. 3(b) and 3(c) are band bending and current components when the laser is focused near the SPCM peak position in Fig. 3(a).

The long minority carrier lifetime indicates a slow electron–hole recombination. This is consistent with the nature of the electronic bands involved in the recombination. In tetrahedrally bonded, direct–band gap semiconductors (e.g., GaAs), the bottom of the conduction band is derived from the atomic s-orbital and the top of the valence band is derived from the atomic p-orbital such that electron–hole recombination can readily occur via an s−p dipole transition. In I phase VO_2, on the contrary, both the valence and the conduction subbands are split from the same atomic orbital, the vanadium $d_{||}$-($d_{x^2-y^2}$) band, as shown schematically in Fig. 1(a). The first-order dipole transition is thus forbidden, and the radiative recombination rate is thus much slower, resulting in a long minority carrier lifetime governed by nonradiative recombination mediated by defects. Further theoretical and experimental work is required to confirm this conjecture.

To study the local band structure associated with the M-I domain walls, SPCM measurements were performed with M domains present in a NB device (D2) at elevated temperatures (Fig. 4). As the temperature was ramped up, the first M domain typically appeared at 55 °C. Multiple M domains nucleated and grew as the temperature was further increased. All M domains eventually merged together, forming a purely M phase NB at a temperature above 100 °C. This domain behavior was explained by substrate-imposed strain effects.[23] Different domain configurations were obtained and stabilized by carefully controlling the NB temperature. Excitation intensity was further reduced to avoid unintentional transitions, and the NBs were monitored optically to ensure that the domain configuration remained the same during the laser scanning. The weak illumination intensity is expected to raise the temperature by ∼0.2 K locally. The M domain has a much lower Seebeck coefficient than that of the I phase, but the M domain is short and the temperature difference across it is ignorable. Therefore, the thermoelectric currents toward the right and the left contacts should still largely cancel each other, as discussed earlier, and can be ignored.

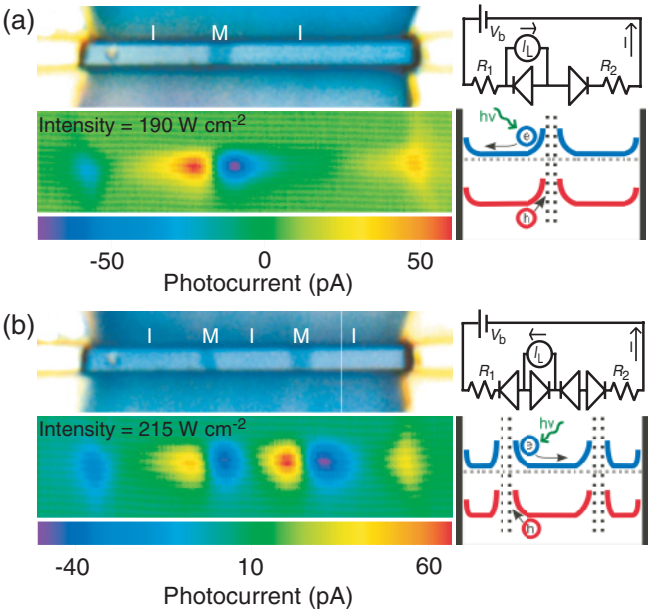

FIG. 4. (Color online) (a) Optical image and zero-bias SPCM image of a VO_2 NB with a single M domain at 55 °C (Device D2). The circuit model and band diagram are shown on the right. (b) Same device with two separate M domains at slightly higher temperature. The positive direction of the current is defined from left to right for both cases.

The SPCM results obtained with one and two M domains are shown in Figs. 4(a) and 4(b), respectively. Photocurrent spots of opposite polarity were seen on each side of an M domain, and the signs of the photocurrent spots were independent of the size and the number of M domains. The photocurrent signs are consistent with an upward band bending toward the M domain (band diagrams shown in Fig. 4). But the linear I-V curve and the reduced resistance with M domains present suggest that the contact resistance at M-I interface is still low compared with the I phase resistance. To our knowledge, this is the first report on the band bending at the M-I domain wall in VO_2. The band bending direction suggests the initial Fermi level of the M phase lies below the Fermi level of the I phase, which is close to the bottom of the conduction band because the I phase is unintentionally highly n-doped.[17] Since both phases of VO_2 are not piezoelectric, strain at the domain wall is not expected to induce an electric field. In addition, the photocurrent decays exponentially in the I phase at 55 °C, consistent with the room temperature measurements [Fig. 4(a)]. The decay length of 2.2 μm (line plot and fitting not shown) is slightly shorter than the length of 3.1–3.5 μm at room temperature in the same device, presumably because of a shorter carrier lifetime at higher temperatures.

To extract the barrier height, we model the VO_2 NB device by an equivalent circuit, treating the M-I interface as a Schottky diode. Each M domain is associated with two

Schottky barriers, equivalent to two diodes connected back to back. Assuming ideal contacts and identical barrier height at each side of the M domain, the single M domain configuration with the excitation on the left domain wall can be modeled by the circuit diagram in Fig. 4(a). The current obeys the following equation:

$$-\frac{kT}{|e|}\ln\left(\frac{I}{I_0}+1\right)+\frac{kT}{|e|}\ln\left(\frac{I_L-I}{I_0}+1\right)+V_b-IR=0, \quad (1)$$

where I_L is the current generated by light, I_0 is the saturation current of an individual diode, V_b is the bias voltage, R is the total NB I phase resistance, k is the Boltzmann constant, T is the temperature, and $|e|$ is the electron charge. If the current is small ($I \ll I_0$ and $I_L - I \ll I_0$), Eq. (1) can be simplified to

$$I=\frac{V_b+kT\,I_L/|e|\,I_0}{R}. \quad (2)$$

Equation (2) predicts a linear relation between I and V_b, consistent with the linear I-V curves measured under local excitation. Taking the experimental values of the short-circuit current $I_{sc} = 60$ pA and $R = 1$ MΩ, we obtain $I_L/I_0 = 0.0023$, which confirms the small current assumption because $I < I_L \ll I_0$. Assuming a 100% internal charge separation efficiency η_{cc} (defined by the fraction of the light generated carrier flux to the absorbed photon flux: $\eta_{cc} = I_L/qF$), we obtained $I_0 = 0.5$ mA. We can then estimate the barrier height ϕ, assuming that the current is dominated by thermionic emission:

$$J_0 = A^* T^2 e^{-\phi/kT}, \quad (3)$$

where A^* is the Richardson constant (proportional to electron effective mass $m_e^* = 60\ m_0$ in VO_2[24]) and J_0 is the saturation current density ($=I_0$/area). By using the I_0 value obtained from the circuit model, the barrier was calculated to be approximately $\phi = 0.28$ eV. This value depends on the η_{cc} logarithmically and is the lower boundary of the actual barrier height. A charge separation efficiency $\eta_{cc} = 100\%$ is expected, because the charge transit time across the injection area is much shorter than the carrier lifetime.[25] Even if $\eta_{cc} = 10\%$ instead of 100%, this only increases the calculated barrier height slightly to $\phi = 0.31$ eV, because the dependence is logarithmic.

The barrier height at the M-I junction is a direct measure of the band offset between the M and the I phases, which is useful for understanding the IMT and has not yet been obtained experimentally. The measured ~0.3-eV barrier height provides direct evidence that the Fermi level of the M phase is near the middle of the band gap ($E_g \approx 0.6 - 0.7$ eV) of the I phase in VO_2. As shown by the schematic band diagram in Fig. 1(a), this indicates a nearly symmetric opening of the $d_{||}$-band into the band gap when the M phase transitions to the I phase. This is consistent with the picture of Mott transition, where the narrow d-band is symmetrically split into the upper and the lower Hubbard subbands. This also indicates that the upward shift of the d_π-band is important, such that its bottom is not much lower than that of the $d_{||}^*$ band [Fig. 1(a)].

The direct identification of a Schottky junction at the M-I domain wall also indicates a space charge region between the coexisting I and M phases. As the band in the I phase bends at the M-I junction, the charge density is greatly reduced in the associated depletion region. In the Mott transition picture, thermal activation increases the charge density (n) to a threshold value and triggers the transition and the consequent crystal structure change.[17,26] Thus, the depletion region at the M-I domain wall effectively presents an energy barrier to the IMT, because additional electrons need to be injected into the depletion region to meet the charge density threshold for the M domain to expand.

IV. CONCLUSIONS

In summary, we have studied the IMT in VO_2 NBs by SPCM. We observed band bending arising from the Schottky junction at the M-I domain wall. The barrier height extracted from the photocurrent indicates that the Fermi level of the M phase lies near the middle of the I phase band gap, suggesting a symmetric band gap opening upon phase transition. We also observed unexpectedly long minority carrier diffusion lengths in the I phase. We attribute the photocurrent to carrier diffusion and extract a long recombination lifetime on the order of microseconds from the SPCM data, which is consistent with a slow carrier recombination across the d-subbands of VO_2.

ACKNOWLEDGMENTS

The SPCM characterization was supported by the University of California at Davis Startup Fund and the Hellman Fellowship. Materials synthesis (J.W.) was supported by a National Science Foundation Career Award under Grant No. DMR-1055938. Modeling (D.F.) was supported by the Graduate Student Research Innovation Project of Jiangsu Province of China (Grant No. CX09B_009Z).

*yu@physics.ucdavis.edu

[1] F. J. Morin, Phys. Rev. Lett. **3**, 34 (1959).
[2] H. W. Verleur, A. S. Barker, and C. N. Berglund, Phys. Rev. **172**, 788 (1968).
[3] N. F. Mott, Rev. Mod. Phys. **40**, 677 (1968).
[4] P. P. Edwards, R. L. Johnston, C. N. R. Rao, D. P. Tunstall, and F. Hensel, Philos. Trans. R. Soc. London Ser. A **356**, 5 (1998).
[5] M. M. Qazilbash, M. Brehm, B.-G. Chae, P. C. Ho, G. O. Andreev, B.-J. Kim, S. J. Yun, A. V. Balatsky, M. B. Maple, F. Keilmann, H.-T. Kim, and D. N. Basov, Science **318**, 1750 (2007).
[6] B. S. Guiton, Q. Gu, A. L. Prieto, M. S. Gudiksen, and H. Park, J. Am. Chem. Soc. **127**, 498 (2004).
[7] Y. Ahn, J. Dunning, and J. Park, Nano Lett. **5**, 1367 (2005).
[8] Y. Gu, J. P. Romankiewicz, J. K. David, J. L. Lensch, and L. J. Lauhon, Nano Lett. **6**, 948 (2006).
[9] Y. H. Ahn, A. W. Tsen, B. Kim, Y. W. Park, and J. Park, Nano Lett. **7**, 3320 (2007).
[10] Y.-J. Doh, K. N. Maher, L. Ouyang, C. L. Yu, and H. Park, Nano Lett. **8**, 4552 (2008).

[11] J. E. Allen, E. R. Hemesath, and L. J. Lauhon, Nano Lett. **9**, 1903 (2009).
[12] R. Graham, C. Miller, E. Oh, and D. Yu, Nano Lett. **11**, 717 (2011).
[13] M. C. Putnam, D. B. Turner-Evans, M. D. Kelzenberg, S. W. Boettcher, N. S. Lewis, and H. A. Atwater, Appl. Phys. Lett. **95**, 163116 (2009).
[14] B. Varghese, R. Tamang, E. S. Tok, S. G. Mhaisalkar, and C. H. Sow, J. Phys. Chem. C **114**, 15149 (2010).
[15] A. Tselev, E. Strelcov, I. A. Luk'yanchuk, J. D. Budai, J. Z. Tischler, I. N. Ivanov, K. Jones, R. Proksch, S. V. Kalinin, and A. Kolmakov, Nano Lett. **10**, 2003 (2010).
[16] J. Cao, W. Fan, H. Zheng, and J. Wu, Nano Lett. **9**, 4001 (2009).
[17] J. Cao, W. Fan, K. Chen, N. Tamura, M. Kunz, V. Eyert, and J. Wu, Phys. Rev. B **82**, 241101 (2010).
[18] D. Fu, J. Zou, K. Wang, R. Zhang, D. Yu, and J. Wu, Nano Lett. **11**, 3809 (2011).
[19] C. N. Berglund and H. J. Guggenheim, Phys. Rev. **185**, 1022 (1969).
[20] See Supplemental Material at http://link.aps.org/supplemental/10.1103/PhysRevB.85.085111 for a temporal photoresponse measurement and more simulation results.
[21] C.-J. Kim, H.-S. Lee, Y.-J. Cho, K. Kang, and M.-H. Jo, Nano Lett. **10**, 2043 (2010).
[22] M. Rini, Z. Hao, R. W. Schoenlein, C. Giannetti, F. Parmigiani, S. Fourmaux, J. C. Kieffer, A. Fujimori, M. Onoda, S. Wall, and A. Cavalleri, Appl. Phys. Lett. **92**, 181904 (2008).
[23] J. Wu, Q. Gu, B. S. Guiton, N. P. de Leon, L. Ouyang, and H. Park, Nano Lett. **6**, 2313 (2006).
[24] A. Zylbersztejn and N. F. Mott, Phys. Rev. B **11**, 4383 (1975).
[25] η_{cc} is determined by the carrier recombination rate k_r and the charge separation rate k_{cc} ($\eta_{cc} = \frac{k_{cc}}{k_{cc}+k_r}$). The carrier recombination rate can be estimated from the inverse of the carrier lifetime $\sim 10^5$ s^{-1}, and the charge separation rate can be estimated from the inverse of the charge transit time $k_{cc} = \frac{D_p}{w^2} = 10^6$ s^{-1}, where we take the laser beam width $w = 1$ μm and the diffusion coefficient $D_p = 0.01$ cm^2/s for $\mu_p = 0.5$ cm^2/Vs.
[26] N. F. Mott, *Metal–Insulator Transitions* (Taylor & Francis, Bristol, 1990).